CHALMERS
FINITE ELEMENT CENTER

PREPRINT 2001–07

Integration methods for the calculation of the magnetostatic field due to coils

Marzia Fontana

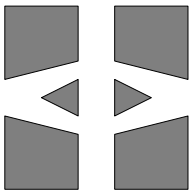

Chalmers Finite Element Center
CHALMERS UNIVERSITY OF TECHNOLOGY
Göteborg Sweden 2001

CHALMERS FINITE ELEMENT CENTER

Preprint 2001–07

Integration methods for the calculation of the magnetostatic field due to coils

Marzia Fontana

CHALMERS

Chalmers Finite Element Center
Chalmers University of Technology
SE–412 96 Göteborg Sweden
Göteborg, April 2001

Integration methods for the calculation of the magnetostatic field due to coils

Marzia Fontana

NO 2001–07
ISSN 1404–4382

Chalmers Finite Element Center
Chalmers University of Technology
SE–412 96 Göteborg
Sweden
Telephone: +46 (0)31 772 1000
Fax: +46 (0)31 772 3595
www.phi.chalmers.se

Printed in Sweden
Chalmers University of Technology
Göteborg, Sweden 2001

Integration methods for the calculation of the magnetostatic field due to coils

Marzia Fontana[1]

Abstract

Analytical and numerical integration methods of the Biot-Savart law are presented for the three-dimensional computation of the magnetic field generated by stationary currents. For complex-shaped conductors a finite volume approximation is proposed, based on a composite Gauss-Legendre quadrature on tetrahedral subdomains of the conductors. For circular coils with rectangular cross section, a modified semi-analytical Urankar's method is considered, expressed in terms of elementary functions, Jacobian elliptic functions and complete/incomplete elliptic integrals of the first, second and third kind. As alternative, numerical integration can be applied to sequences of one-dimensional non-singular integrals in azimuthal coordinate. For massive computation on a large number of field points, an optimized integration scheme for coils is suggested, by combining the modified Urankar's method with one-dimensional numerical integration. Numerical examples are reported on significant test cases for a comparison among the several integration methods proposed.

Key words - Elliptic integrals, Jacobian elliptic functions, finite volume approximation, magnetic fields, Biot-Savart law.

1 Introduction

Mathematics is a necessary tool for physical and engineering applications in the twofold activity of *modelling* (formulation of problems through models) and *comput tion* (model solution through analytical and numerical methods). As an important engineering application resorting to mathematical methods, we here consider the problem of large scale magnetic field computation, which leads to the mathematical problem of analytical and numerical three-dimensional integration over complex-shaped conducting domains.

A vast amount of problems and devices around us can be explained by analysis of electromagnetic fields: cathode-ray oscilloscopes, television reception, radar, satellite/mobile and optical fiber communication, microwave devices, remote sensing, radio astronomy, brain

[1]E-mail address: *marzia@math.chalmers.se, marzia@iname.com*
Department of Mathematics, Chalmers University of Technology, S-412 96 Göteborg, Sweden.
Work supported by CNR research fellowship 203.01.70, Consiglio Nazionale delle Ricerche, Italy
2000 Mathematics Subject Classification: 65D30, 78A25, 78A35

scanners, electromagnetic shielding, particle accelerators, MRI for real life systems, and so on. In the design of electromagnetic devices and in the prediction of electromagnetic phenomena, the analysis needs to be carried out with accurate computation of source and induced electro-magnetic fields, taking into account several aspects: the physical properties of the materials, the geometric shapes and constraints, the boundary/interface conditions, the magnitude of involved forces, the knowledge of source currents with determination of its critical limits, and electromagnetic induction phenomena.

The computation of the magnetic field due to source currents is a fundamental task in many electromagnetic problems as an autonomous physical datum and, moreover, as a "partial" information inserted into a differential model representing a specific electromagnetic problem. In fact, mathematical models based on Maxwell's equations, the fundamental differential equations governing all macroscopic electromagnetic phenomena, can lead to (initial) boundary value problems where the source magnetic field appears as a datum in the right hand side contribution of the differential equations or as a quantity in implicit form in the interface and boundary conditions [12]. In this case the source magnetic field has to be estimated during the initial modelling phase preceding the effective model solution.

The contribution of this work is, therefore, to present some analytical and numerical methods for the computation of the magnetic field contribution generated by source currents, resorting to the two basic physical integral laws - Ampere's circuital law and the Biot-Savart law - which define it, the former implicitly and the latter explicitly. Because of the explicit definition of the source field, and due to the presence of a singularity of type $O(|\mathbf{r}-\mathbf{r}'|^{-3})$ in the integrand function, which makes the integral interesting from a mathematical point of view, the Biot-Savart law will be the integral mainly investigated here. The suggested integration methods take into consideration the shape of the current-carrying conductor. While for complex-shaped conductors only numerical or semi-numerical integration techniques are possible, for particular coil geometries an analytical approach can be used, resorting to computation of Jacobian elliptic functions and complete/incomplete elliptic integrals of the first, second and third kind.

The report is organized as follows.

Section 2 is a brief introduction about the main electromagnetic laws, like Maxwell's equations, constitutive relations and boundary conditions.

Section 3 presents an overview of the main integration methods that have been investigated in the literature for the computation of Ampere's law and, especially, some numerical integration techniques that can be applied to the Biot-Savart law.

Section 4 discusses the case in which the current-carrying conductor is a circular coil with rectangular cross section, for which a semi-analytical integration of the Biot-Savart

law can be derived. Regarding this, notice that Urankar's method has been already investigated in the literature: the purpose of the section is rather to correct some wrong values reported in previous references, to specify values for limit field positions not originally considered, and to improve the computational efficiency of the method for a massive computation on a large number of field points (as it occurs, for instance, in finite element computations). A mixed numerical and semi-analytical approach is suggested to improve accuracy in points on the conductor boundary.

An analysis of results on test cases is finally provided in Section 5. Numerical comparisons in terms of accuracy and computational time are done among the modified Urankar's semi-analytical method, a numerical quadrature of one-dimensional integrals in azimuthal coordinate, and a finite volume approximation with composite Gaussian integration over subdomains of the current-carrying regions.

2 Fundamental laws in electromagnetism

The fundamental equations governing electromagnetic phenomena are the well-known *M xwell's equ tions*. For all space points, in the general time dependent case they can be written as

$$\nabla \times \mathbf{E} + \frac{\partial \mathbf{B}}{\partial t} = 0 \tag{2.1}$$

$$\nabla \times \mathbf{H} - \frac{\partial \mathbf{D}}{\partial t} = \mathbf{J}, \tag{2.2}$$

called *F r d y-Henry's* and *M xwell-Ampere's l w* respectively, together with

$$\nabla \cdot \mathbf{D} = \rho \tag{2.3}$$

$$\nabla \cdot \mathbf{B} = 0, \tag{2.4}$$

called *G uss's* and *m gnetic G uss's l w*, where $\mathbf{E}$ is the electric field intensity, $\mathbf{D}$ is the electric flux density, $\mathbf{H}$ is the magnetic field intensity, $\mathbf{B}$ is the magnetic flux density, $\mathbf{J}$ is the electric current density, and ρ is the electric charge volume density. In the international system SI the following measure units are used: [$\mathbf{E}$]=volts/meter, [$\mathbf{D}$]=coulombs/meter^2, [$\mathbf{H}$]=amperes/meter, [$\mathbf{B}$]=webers/meter^2, [$\mathbf{J}$]=amperes/meter^2 and [ρ]=coulombs/meter^3.

Generally, Maxwell's equations are considered together with the fundamental relation (*equ tion of continuity*)

$$\nabla \cdot \mathbf{J} + \frac{\partial \rho}{\partial t} = 0, \tag{2.5}$$

which specifies the conservation of charge. Only three of the five equations (2.1)-(2.4) and (2.5) are independent. Generally they are assumed to be Faraday-Henry's law, Maxwell-Ampere's law and the equation of continuity, since Gauss' s law both in the electric and in the magnetic form can be derived from them.

Maxwell's equations become a definite system of equations when *constitutive rel tions* describing the macroscopic properties of the materials are considered. For a simple medium they are

$$\mathbf{J} = \sigma\mathbf{E} + \mathbf{J}_s \tag{2.6}$$

$$\mathbf{D} = \epsilon\mathbf{E} \tag{2.7}$$

$$\mathbf{B} = \mu\mathbf{H}, \tag{2.8}$$

where $\mathbf{J}_s$ is the imposed source current density, σ is the electric conductivity, ϵ is the electric permittivity and μ is the magnetic permeability of the medium. The constitutive parameters σ, ϵ and μ are tensors for anisotropic media, scalars for isotropic media and they are functions of space for inhomogeneous media. Besides, for lossy media they are complex-valued.

Depending on the properties of the considered material, the permeability μ in equation (2.8) can also be function of the field intensity $\mathbf{H}$. If not, i.e. $\mathbf{B}$ and $\mathbf{H}$ are linearly related, the material is called *line r*. For permanent magnets equation (2.8) assumes the modified form

$$\mathbf{B} = \mu(\mathbf{H} - \mathbf{H}_c), \tag{2.9}$$

where $\mathbf{H}_c$ is the *coercive field intensity* (i.e. the reverse magnetic field intensity that has to be applied to reduce magnetization to zero). In most cases, it is assumed that the relationship between $\mathbf{B}$ and $\mathbf{H}$ is linear even for a permanent magnet. Generally, definitions $\epsilon = \epsilon_r\epsilon_0$ and $\mu = \mu_r\mu_0$ are used, with reference to the corresponding permeability $\mu_0 = 4\pi\,10^{-7} H/m$ (henry/meter) and permittivity $\epsilon_0 = 1/(c_0^2\mu_0) \approx 10^{-9}/(36\pi) F/m$ (farad/meter, where c_0 is the speed of light) in free space. μ_r and ϵ_r are dimensionless values associated to the material, called *rel tive permittivity* and *rel tive perme bility.*

(*Electrost tic/m gnetost tic c se*) When the field quantities do not vary with time, electric and magnetic properties decouple from each others and Maxwell's equations reduce to two independent systems:

$$\nabla \times \mathbf{E} = 0 \tag{2.10}$$

$$\nabla \cdot \mathbf{D} = \rho$$

for the electrostatic case, and

$$\nabla \times \mathbf{H} = \mathbf{J} \tag{2.11}$$

$$\nabla \cdot \mathbf{B} = 0$$

for the magnetostatic case. The static equation of continuity

$$\nabla \cdot \mathbf{J} = 0 \tag{2.12}$$

is an immediate consequence of the first relation in (2.11).

(*Qu si-st tic c se*) In the time dependent case, if the time variation is sufficiently slow we can neglect the *displ cement current* $\partial \mathbf{D}/\partial t$ in (2.2). This hypothesis leads to the so-called *qu si-st tic pproxim tion*. Differently from the static case, nevertheless, the variation of the magnetic flux density $\mathbf{B}$ is not negligible and Faraday-Henry's equation (2.1) remains unchanged like in the time-dependent general case. Analogously to static situations, equation (2.12) holds. The quasi-static assumption is valid for problems in which frequencies are low or, more precisely, when the size of the structure is small compared with the electromagnetic wavelength associated to the highest frequency component occurring in the problem.

(*Bound ry nd interf ce conditions*) To find the actual solution of a specific electromagnetic problem, Maxwell's equations have to be accompanied by boundary conditions associated to the space domain together with initial conditions in the time dependent case. In addition, interface conditions between materials have to be considered, describing the transmission of fields from one material to the other. Given two contiguous media i and j, corresponding to the disjoint domains Ω_i and Ω_j, such that $\partial\Omega_i \cap \partial\Omega_j = \Gamma_{ij} \neq \emptyset$, the transmission conditions at Γ_{ij} can be expressed as

$$\mathbf{n} \times (\mathbf{E}_i - \mathbf{E}_j) = 0 \tag{2.13}$$
$$\mathbf{n} \times (\mathbf{H}_i - \mathbf{H}_j) = \mathbf{J}_{surf} \tag{2.14}$$
$$\mathbf{n} \cdot (\mathbf{D}_i - \mathbf{D}_j) = \rho_{surf} \tag{2.15}$$
$$\mathbf{n} \cdot (\mathbf{B}_i - \mathbf{B}_j) = 0 \tag{2.16}$$

where $\mathbf{n}$ is the unit vector normal to Γ_{ij} pointing from Ω_j into Ω_i, and the quantities ρ_{surf} and $\mathbf{J}_{surf}$ are the surface charge density and the surface electric current density, respectively. The first two conditions give information about the *t ngenti l* component of the fields $\mathbf{E}$ and $\mathbf{H}$: the former is continuous, the latter is discontinuous if surface currents exist. The last two conditions describe the *norm l* component of $\mathbf{D}$ and $\mathbf{B}$, respectively discontinuous, if surface charges exist, and continuous.

Of these four conditions only two are independent, for instance (2.13) and (2.14). The condition (2.13) for the tangential component of $\mathbf{E}$ is equivalent to the condition (2.16) for the normal component of $\mathbf{B}$, while the condition (2.14) for the tangential component of $\mathbf{H}$ corresponds to (2.15) for the normal component of $\mathbf{D}$. In the quasi-static approximation, where $\nabla \cdot \mathbf{J} = 0$, also the condition

$$\mathbf{n} \cdot (\mathbf{J}_i - \mathbf{J}_j) = 0 \tag{2.17}$$

has to be considered, describing the continuity of the normal component of the current density at the interface Γ_{ij}.

Given a bounded material domain Ω, conditions at the boundary $\Gamma = \partial\Omega$ have to be modelled analogously to (2.13)-(2.16) considering that what is mathematically a "boundary" is nothing but an interface with an *extern l* medium whose electromagnetic status is already known. This means that fields or their normal or tangential components are assigned data on the several parts of Γ. Boundary data have, of course, to be given in a consistent way so that they are compatible with each other.

For a more detailed overview of electromagnetic theory, see [10, 13, 19].

3 Computation of the source magnetic field by Ampere's and Biot-Savart laws

The total magnetic field intensity can be considered as the sum of two different contributions, one generated by imposed source currents and the other due to induced magnetization of the background materials. The rigorous argument is Helmhotz's theorem, which asserts that the magnetic field intensity $\mathbf{H}$ can be always partitioned as

$$\mathbf{H} = \mathbf{H}_s + \mathbf{H}_m, \tag{3.1}$$

where $\mathbf{H}_s$ is solenoidal (the magnetic field intensity due to prescribed currents), while $\mathbf{H}_m$ is irrotational (the magnetic field intensity due to induced magnetization). The source field $\mathbf{H}_s$ can be computed by using the *Biot-S v rt l w.* Consider an open domain $\Omega \subseteq \mathbb{R}^3$. Given a source current density $\mathbf{J}_s$ defined on a region $\Omega_s \subseteq \Omega$, called *source region*, such law tells that for any point $\mathbf{r} \in \Omega$ the resulting field $\mathbf{H}_s = \mathbf{H}_s(\mathbf{r})$ is given by

$$\mathbf{H}_s = \frac{1}{4\pi} \int_{\Omega_s} \mathbf{J}_s \times \nabla\Big(\frac{1}{|\,\mathbf{r} - \mathbf{r}'\,|}\Big)\, d\mathbf{r}' \tag{3.2}$$

where $\mathbf{r}'$ denotes any point in Ω_s (called *source point*).

Another approach could be to define implicitly the source field by Ampere's circuital law. This one can be easily obtained in its integral form by applying Stoke's theorem to the static source relation $\nabla \times \mathbf{H}_s = \mathbf{J}_s$, giving raise to

$$\oint_{\gamma} \mathbf{H}_s \cdot d\ell = \int_{\mathcal{S}} \mathbf{J}_s \cdot d\mathcal{S} \tag{3.3}$$

for any closed piecewise regular path $\gamma \subseteq \Omega$, being $\mathcal{S}$ a piecewise regular surface such that $\partial\mathcal{S} = \gamma$ [10, 13].

These laws represent the main subject of study in the present work. The purpose, in fact, is to investigate several numerical and analytical methods that can be used to compute the magnetic field intensity $\mathbf{H}_s$ due to imposed currents, resorting to integration of Ampere's circuital law (3.3) or the Biot-Savart law (3.2).

Regarding this, notice that a possible drawback in Ampere's law is the implicit form of $\mathbf{H}_s$ definition. However, many methods have been investigated in the literature for a numerical estimation of (3.3). In some cases, the source magnetic field has to be estimated as a modelling datum inside a more extended electromagnetic problem, e.g. a boundary value problem by potential formulation in the frame of a finite element computation. In this case, a typical choice of curves γ and surfaces $\mathcal{S}$ is to use sequences of edges (trees) and faces (loops of faces) of the elements used in the associated finite element mesh. This 'discrete' choice of curves through edge-trees derived from the finite element mesh can then represent a successive advantage because information can be reused for the computation of specific line integrals of $\mathbf{H}_s$ obtained as data for the interface and boundary conditions of Dirichlet type. A description of some techniques for the numerical integration of Ampere's circuital law, as well as the Biot-Savart law, is contained in [18] and references quoted therein.

The present work rather focuses on Biot-Savart's integral, giving an explicit $\mathbf{H}_s$ definition. Expression (3.2) can, equivalently, be written as

$$\mathbf{H}_s(\mathbf{r}) = \frac{1}{4\pi} \int_{\Omega_s} \mathbf{J}_s \times \frac{\mathbf{r} - \mathbf{r}'}{\mid \mathbf{r} - \mathbf{r}' \mid^3} \quad d\mathbf{r}', \tag{3.4}$$

where Ω_s is the source region, $\mathbf{r}$ is an arbitrary point in space (called *field point*) and $\mathbf{r}'$ is any source point.

Different methods for the computation of the Biot-Savart law have been developed by many authors. Some of them require assumptions and restrictions on the shape of the source regions (e.g. coils and bars with particular cross sections) or the current density $\mathbf{J}_s$ (e.g. constant in magnitude). Among the numerical approaches, in the so-called *fil ment pproxim tion* the source region is a coil whose cross-sectional area is negligible, while in the *sheet pproxim tion*, it is the thickness of the coil to be negligible. These methods can then be applied to current-carrying conductors having more general shape by splitting them in finite filaments or finite sheets, and mixed approaches can be used according to the local geometry. A more efficient and faster semi-analytical approach that can be used with coils, as suggested by Ciric in [11], is the so-called *surf ce source pproxim tion*, based on formulas containing only elementary functions, in which the coil is approximated by the union of straight segments having rectangular or polygonal cross sections whose

faces along the current directions are trapezoidal. When coils have a big inner radius, the method is faster and more accurate than the above mentioned techniques. On the other hand, when coils have high curvature the segment decomposition has to be chosen finer, with consequent increase of the computational cost and time.

For more general current-carrying geometries the *finite volume pproxim tion* is suggested, based on subdivision of the domain into small elements (the so-called finite volumes). On each volume domain a numerical integration scheme with a proper order (typically, a Gauss-Legendre quadrature) is applied, and contributions from all elements are then summed up. If the Biot-Savart law needs to be computed in the context of magnetostatic boundary value problems to be solved by finite element methods (see for instance [12]), the efficiency of this finite volume approach can be tested by choosing as small volumes the elements of the domain triangulation used for the finite element model. In such a case, it is required that the current-carrying regions are modelled by the mesh generator, i.e. the triangulation is constrained to the boundary of the current-carrying conductors. Anyway, although this method allows to compute the Biot-Savart law for any shape of the source region, a possible drawback is that it is quite time and memory consuming when a large number of volumes is used to increase the accuracy of the computed $\mathbf{H}_s$ values. Besides, in the finite volume approximation as well as in all techniques performed by numerical integration, a particular care is required when points $\mathbf{r}$ in field regions approach points $\mathbf{r}'$ in source regions, because of the singularity $1/\mid \mathbf{r}-\mathbf{r}' \mid^3$ in the integrand function of (3.4). In Section 5 we are going to say something more about these numerical aspects.

In order to overcome these drawbacks of the numerical integrations, an alternative method is suggested by Urankar [20, 21, 22, 23, 24, 25, 26] based on a sequence of analytical formulas, which are valid for various types of current-carrying geometries. This method has been fairly investigated in the literature: equivalent expressions of Urankar's formulas can be found, for instance, in [2, 3, 15]. As these formulas have been implemented for our test-problems, their analytical expression is presented (and corrected) in the next section, for the significant case in which the current-carrying conductor is a circular coil with rectangular cross section.

4 Analytical integration of the Biot-Savart law for coils with rectangular cross section

In real electromagnetic devices, current-carrying regions have mainly the shape of coils whose geometry may be made, in general, of finite circular arcs and/or straight segments. The magnetic source field due to the current is then obtained by summing up the partial fields generated by each part. For all the basic coil geometries (circular filaments, cylinders, coils with rectangular or n-sided polygonal cross sections) Urankar has given an analytical

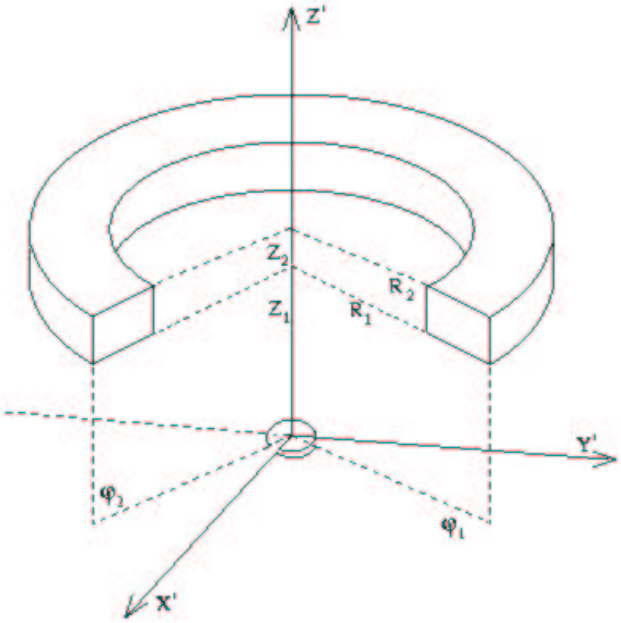

Figure 1: Circular coil with rectangular cross section

representation of the source field $\mathbf{H}_s$ in terms of elementary functions, Jacobian elliptic functions and complete/incomplete elliptic integrals of the first, second and third kind. Urankar's results are here reported for a current-carrying region having the shape of a circular torus with rectangular cross section, or an azimuthal restriction of it [22], as they have been used in the magnetostatic models studied in [12]. For implementation purposes, we also suggest a slightly modified semi-numerical version of Urankar's procedure in order to improve the efficiency of the method when it has to be applied on a large number of field points located in arbitrary positions with respect to the coil. Following an analogous procedure, similar formulas can be derived also to compute the magnetic vector potential $\mathbf{A}$ and, moreover, a generalization for coils having n-sided polygonal cross section can be obtained. A description of such generalization is contained in [24].

Consider in (3.4) an azimuthal source current density $\mathbf{J}_s$, constant in magnitude, whose domain Ω_s is the circular torus with rectangular cross section given by

$$\Omega_s = \{(r', \varphi', z') : \ R_1 \leq r' \leq R_2, \ \varphi_1 \leq \varphi' \leq \varphi_2, \ Z_1 \leq z' \leq Z_2\} \tag{4.1}$$

being known the radii R_1 and R_2, the angles φ_1 and φ_2, and the heights Z_1 and Z_2 (see Figure 1). For the following let $\mathbf{r}' = (r', \varphi', z')$ denote the generic source point, and $\mathbf{r} = (r, \varphi, z)$ the generic field point. For physical reasons it is always $-\pi \leq \varphi \leq \pi$ and,

without any loss of generality, it is possible to assume $-2\pi \le \varphi_1 \le \varphi_2 \le 2\pi$. Rewriting in cylindrical coordinates, after integration over r' and z', the source magnetic field intensity $\mathbf{H}_s$ can be written as

$$\mathbf{H}_s(r,\varphi,z) = \frac{J_s}{4\pi}\big(\widetilde{\mathbf{H}}(R_2,\varphi,Z_2) - \widetilde{\mathbf{H}}(R_1,\varphi,Z_2) + \widetilde{\mathbf{H}}(R_2,\varphi,Z_1) - \widetilde{\mathbf{H}}(R_1,\varphi,Z_1)\big), \qquad (4.2)$$

where the cylindrical components of $\widetilde{\mathbf{H}}$ are given by

$$\begin{aligned}
\widetilde{H}_r(r,\varphi,z) &= \int_{\vartheta_1}^{\vartheta_2} \cos\vartheta \left(D(\vartheta) + r\cos\vartheta \ \sinh^{-1}\beta_1(\vartheta)\right) d\vartheta \\
\widetilde{H}_\vartheta(r,\varphi,z) &= \int_{\vartheta_1}^{\vartheta_2} \sin\vartheta \left(D(\vartheta) + r\cos\vartheta \ \sinh^{-1}\beta_1(\vartheta)\right) d\vartheta, \qquad (4.3)\\
\widetilde{H}_z(r,\varphi,z) &= \int_{\vartheta_1}^{\vartheta_2} (\gamma \ \sinh^{-1}\beta_1(\vartheta) - r\cos\vartheta \sinh^{-1}\beta_2(\vartheta) - r\sin\vartheta \arctan\beta_3(\vartheta))\, d\vartheta
\end{aligned}$$

with the definitions

$$\begin{aligned}
&\gamma = z' - z, \quad \vartheta = \varphi' - \varphi, \quad \vartheta_i = \varphi - \varphi_i \quad \text{for } i = 1,2,\\
&B^2(\vartheta) = r'^2 + r^2 - 2rr'\cos\vartheta, \qquad D^2(\vartheta) = \gamma^2 + B^2(\vartheta),\\
&G^2(\vartheta) = \gamma^2 + r^2\sin^2\vartheta, \qquad \beta_1(\vartheta) = (r' - r\cos\vartheta)/G(\vartheta), \qquad (4.4)\\
&\beta_2(\vartheta) = \gamma/B(\vartheta), \qquad \beta_3(\vartheta) = \gamma(r' - r\cos\vartheta)/(r\sin\vartheta D(\vartheta)).
\end{aligned}$$

Note that in (4.3) terms do not become singular or indeterminate when $\varphi' = \varphi$. Let us substitute then $\alpha = (\pi - \vartheta)/2$, and $\alpha_i = (\pi - \vartheta_i)/2$. Considering in (4.3) the presence of odd and even integrands, the source field can be rewritten in the compact form

$$\widetilde{H}_l(r,\varphi,z) = \sum_{i=1}^{2} (-1)^{i+1}(\delta_{l\varphi} + \delta_{lm}\mathrm{sgn}\,\alpha_i)\,\widehat{H}_l(r,|\,\alpha_i\,|,z), \quad l = r,\varphi,z, \qquad (4.5)$$

with $m = l$ if $l = r, z$ and $m \neq l$ if $l = \varphi$, where δ_{ij} denotes the Kronecker symbol. The expression of functions $\widehat{H}_l$ is given in the following.

First, let us introduce the notation for the *incomplete* elliptic integrals of the first, second and third kind, with argument ϑ, modulus k and characteristic n (see [1, 6, 7, 8]). For any real k such that $-1 < k < 1$, they are defined as the functions $E(\vartheta,k)$, $F(\vartheta,k)$ and $\Pi(\vartheta,n,k)$ respectively, such that

$$
\begin{aligned}
E(\vartheta,k) &= \int_0^{\vartheta} (1-k^2\sin^2\phi)^{1/2}\,d\phi \\
F(\vartheta,k) &= \int_0^{\vartheta} \frac{1}{(1-k^2\sin^2\phi)^{1/2}}\,d\phi \\
\Pi(\vartheta,n,k) &= \int_0^{\vartheta} \frac{1}{(1-n\sin^2\phi)(1-k^2\sin^2\phi)^{1/2}}\,d\phi.
\end{aligned}
\tag{4.6}
$$

where $E(k)=E(\pi/2,k)$, $F(k)=F(\pi/2,k)$ and $\Pi(n,k)=\Pi(\pi/2,n,k)$ are the so-called *complete* elliptic integral of the first, second and third kind, having argument $\pi/2$ and modulus k. Notice that in the definition of the integrals E, F and Π a notation coherent with Abramowitz and Stegun [1] has been here used, i.e. the sign for the parameter n in the integral $\Pi(\vartheta,n,k)$ is opposite to the one used by Bulirsch [6, 7]. Let us then define $\mathrm{sn}\,u$, $\mathrm{cn}\,u$ and $\mathrm{dn}\,u$ as the three basic Jacobian elliptic functions [1, 16] with amplitude $\mathrm{am}\,u = |\,\alpha\,|$ and $\mathrm{am}\,u_i = |\,\alpha_i\,|$, modulus k being implicit, i.e. such that

$$
\begin{aligned}
&\mathrm{sn}\,u = \sin\alpha, && \mathrm{sn}\,u_i = \sin\alpha_i, \\
&\mathrm{cn}\,u = \cos\alpha, && \mathrm{cn}\,u_i = \cos\alpha_i, \\
&\mathrm{dn}\,u = (1-k^2\sin^2\alpha)^{1/2}, && \mathrm{dn}\,u_i = (1-k^2\sin^2\alpha_i)^{1/2}.
\end{aligned}
\tag{4.7}
$$

Under these premises, two cases have then to be distinguished. By the initial assumption $-2\pi \le \varphi' \le 2\pi$, it follows $-\pi \le \alpha, \alpha_i \le 2\pi$. First, let us consider the case $|\,\alpha_i\,| \le \pi/2$, describing a field point whose azimuthal coordinate lies internally to the azimuthal width of the coil arc. Evidently, if the coil describes a complete 2π angle this condition is satisfied for all field points. Then, a double integration by parts of (4.3) is done when the argument is $|\,\alpha_i\,|$. After some trigonometric transformations and rearrangement algebra, it is possible to obtain a form that can be easily rewritten in terms of elliptic integrals and Jacobian elliptic functions, the first ones resulting in fact to be defined in the chosen range for $|\,\alpha_i\,|$. Regarding this, we introduce $c^2=\gamma^2+r^2$, $b=r+r'$, $a^2=\gamma^2+b^2$, $k^2=4rr'/a^2$, and the parameters $n_1=2r/(r-c)$, $n_2=2r/(r+c)$, and $n_3=4rr'/b^2$, together with the function

$$
v(k) = \frac{1+k^2(\gamma^2-br)}{2rr'},
\tag{4.8}
$$

and define $\theta_i = |\,\alpha_i\,|$. Then, terms $\widehat{H}_l$ in (4.5) can be expressed as

$$
\begin{aligned}
\widehat{H}_r(r,\theta_i,z) &= D_r(\theta_i) + r\Im(\theta_i) - \frac{a}{2r}r'[E(\theta_i,k) - v(k)F(\theta_i,k)] \\
&\quad - \frac{1}{4ar}\sum_{p=1}^{3}(-1)^p Q_r(n_p)\Pi(\theta_i,n_p,k) + 2r\,\mathrm{sn}\,u_i\,\mathrm{cn}\,u_i\,\mathrm{dn}\,u_i \\
\widehat{H}_\varphi(r,\theta_i,z) &= D_\varphi(\theta_i) + 2\gamma\Im(\theta_i) - \frac{a}{2r}\,\mathrm{dn}\,u_i(b - 2r\,\mathrm{sn}^2\,u_i) \\
&\quad - \frac{1}{4ar}\sum_{p=1}^{3}(-1)^p Q_\varphi(n_p)I(n_p) \\
\widehat{H}_z(r,\theta_i,z) &= D_z(\theta_i) + 2\gamma\Im(\theta_i) - \frac{3a}{4r}\gamma k^2 F(\theta_i,k) \\
&\quad - \frac{1}{4ar}\sum_{p=1}^{3}(-1)^p Q_z(n_p)\Pi(\theta_i,n_p,k)
\end{aligned}
\tag{4.9}
$$

where

$$
I(n_p) = n_p\int_0^{u_i}\frac{\mathrm{sn}\,u\,\mathrm{cn}\,u\,du}{1 - n_p\,\mathrm{sn}^2\,u}, \tag{4.10}
$$

whose analytical representation in terms of Jacobian elliptic functions is given by

$$
I(\xi) = \begin{cases}
-\frac{|\xi|^{1/2}}{2(k^2-\xi)^{1/2}}\,\ln\frac{[(k^2-\xi)^{1/2}-|\xi|^{1/2}\mathrm{dn}\,u]^2}{1-\xi\,\mathrm{sn}^2 u}, & \xi<0, \\
\frac{1}{\mathrm{dn}\,u}, & \xi>0,\ \xi=k^2, \\
\frac{\xi^{1/2}}{2(\xi-k^2)^{1/2}}\,\ln\frac{[(\xi-k^2)^{1/2}+\xi^{1/2}\,\mathrm{dn}\,u]^2}{1-\xi\mathrm{sn}^2 u}, & \xi>0,\ \xi>k^2, \\
-\frac{\xi^{1/2}}{2(k^2-\xi)^{1/2}}\,\arcsin\frac{2\xi^{1/2}\mathrm{dn}\,u(k^2-\xi)^{1/2}}{k^2\ |1-\xi\,\mathrm{sn}^2 u|}, & \xi>0,\ \xi<k^2,
\end{cases}
\tag{4.11}
$$

The other terms appearing in (4.9) are defined as follows. Defining $\tilde{\beta}_i(\alpha) = \beta_i(\pi - 2\alpha)$ for $i = 1,2,3$, we have

$$
\Im(\alpha) = \int_0^{\alpha}\sinh^{-1}\tilde{\beta}_1(\alpha)d\alpha, \tag{4.12}
$$

$$
D_l(\alpha) = \begin{cases}
\frac{1}{4}r\sin 4\alpha\sinh^{-1}\tilde{\beta}_1(\alpha) \\
\frac{1}{4}r\cos 4\alpha\sinh^{-1}\tilde{\beta}_1(\alpha), & l = r,\varphi,z, \\
r\sin 2\alpha\sinh^{-1}\tilde{\beta}_2(\alpha) + r\cos 2\alpha\tan^{-1}\tilde{\beta}_3(\alpha)
\end{cases}
\tag{4.13}
$$

$$
Q_l(n_p) = \delta_{pq}[r' - (-1)^p c]R_l(n_p) + \delta_{p3}\delta_{lz}\gamma b(r'-r)n_p, \quad l = r,\varphi,z, \tag{4.14}
$$

with $q = p$, if $p = 1, 2$, and

$$R_l(n_p) = \begin{cases} n_p \gamma^2 c/r \\ (-1)^p (c^2 + \gamma^2), \qquad l = r, \varphi, z. \\ -2\gamma c\, n_p, \end{cases} \tag{4.15}$$

In the computations, since $n_1 \to -\infty$ for field points having $\gamma = 0$, i.e. $z = z'$, consider in (4.9) the limit values $\lim_{z \to z'} Q_r(n_1(z)) = 0$ and $\lim_{z \to z'} Q_z(n_1(z)) = 0$.

Let us consider now the second case, when $|\,\alpha_i\,| > \pi/2$, for which the above elliptic integrals are not defined. The following integration domains are distinguished: $\pi/2 < |\,\alpha_i\,| \leq \pi$, $\pi < \alpha_i \leq 3\pi/2$ and $3\pi/2 < \alpha_i \leq 2\pi$. In the two first ranges, we can define $\theta_i = \pi - |\,\alpha_i\,|$, while in the last one $\theta_i = 2\pi - \alpha_i$, so that again $0 < |\,\theta_i\,| \leq \pi/2$. By splitting the domains and using symmetry properties of the corresponding integrands, one easily gets

$$\begin{aligned} &\widehat{H}_\varphi(|\,\alpha_i\,|) = \widehat{H}_\varphi(|\,\theta_i\,|), \\ &\widehat{H}_l(|\,\alpha_i\,|) = \begin{cases} 2\widehat{H}_l(\pi/2) - \operatorname{sgn}\theta_i\, \widehat{H}_l(|\,\theta_i\,|), & \pi/2 < |\,\alpha_i\,| \leq 3\pi/2, \\ 4\widehat{H}_l(\pi/2) - \widehat{H}_l(\theta_i), & 3\pi/2 < \alpha_i \leq 2\pi, \end{cases} \end{aligned} \tag{4.16}$$

for $l = r, z$.

Formulas (4.9) can be simplified in the axisymmetric case. When the coil has the total azimuthal length 2π radians, the φ-component of $\widehat{\mathbf{H}}$ vanishes, while both its r- and z-components do not depend on the angle φ. Therefore, choosing arbitrarily the value of φ, e.g. $\varphi = 0$, and thus $\alpha_i = \pm\pi/2$ for $i = 1, 2$, and considering that $D_r(\pi/2) = 0$, equations (4.9) reduce to

$$\begin{aligned} &\widehat{H}_r(r, \pi/2, z) = r\Im(\pi/2) - \frac{a}{2r} r'[E(k) - v(k)F(k)] - \frac{1}{4ar} \sum_{p=1}^{3} (-1)^p Q_r(n_p) \Pi(n_p, k) \\ &\widehat{H}_\varphi(r, \pi/2, z) = 0 \\ &\widehat{H}_z(r, \pi/2, z) = D_z(\pi/2) + 2\gamma\Im(\pi/2) - \frac{3a}{4r}\gamma k^2 F(k) - \frac{1}{4ar} \sum_{p=1}^{3} (-1)^p Q_z(n_p) \Pi(n_p, k) \end{aligned} \tag{4.17}$$

being $E(k)$, $F(k)$ and $\Pi(n_p, k)$ the complete elliptic integral of the first, second and third kind with argument $\pi/2$ and modulus k, and

$$D_z(\pi/2) = -\pi r/2 \, \operatorname{sgn}\gamma \, [1 + \operatorname{sgn}(r' - r)]. \tag{4.18}$$

In case the field point is located on the z axis, i.e. $r = 0$, the expression of the source field is reduced to

$$\widehat{H}_r(0,\pi/2,z) = \widehat{H}_\varphi(0,\pi/2,z) = 0, \quad \widehat{H}_z(0,\pi/2,z) = \pi\ |\gamma|\ \sinh^{-1}(r'/\gamma). \tag{4.19}$$

Regarding these last expressions, it has to be remarked that in (4.18) the term $\mathrm{sgn}(\pm\pi/2)$ (miss-print) has been removed from (22c) in [22], while in (4.19) $|\gamma|$ has been corrected at place of γ appearing in (23) of [22]. In the computations, moreover, for field points having $\gamma = 0$, i.e. $z = z'$, consider the limit value $\lim_{z\to z'} \widehat{H}_z(0,\pi/2,z) = 0$.

Except for the integral $\Im(\alpha)$ in (4.12), the above formulas have all been expressed in terms of elementary functions, Jacobian elliptic functions and elliptic integrals. Since the Jacobian elliptic functions can be reduced to trigonometric functions by (4.7), also the expression (4.11) for the integral $I(n_p)$ is known analytically. Many efficient algorithms exist for the computation of the elliptic integrals of the first, second kind and third kind. Classical approaches, well known from the literature, are the Landen transformation for incomplete integrals of the first kind, the Bartky transformation for integrals of the second kind and Bulirsch's extension to integrals of the third kind [6, 7, 8]. Another more recent method, used in the present work, is the unified Carlson's algorithm valid for all three integrals, as it is suggested in [17]. An advantage of Carlson's procedure is that the cancellation errors occurring in the previous methods are reduced in a significant way.

Moreover, these formulas are valid for all field positions. For implementation purposes, a particular care has rather to be used in the choice of the algorithm for the computation of the elliptic integrals. A straightforward application of Carlson's algorithm, for instance, even if it is more precise than the other methods, turns out to be not defined for special points, corresponding to the limit positions (called *critic curves*) $z = Z_i$ and $r = R_i$, or $z = Z_i$ and $r = r_i^\star$, where $r_i^\star = R_i/(4R_i - 1)$, $i = 1, 2$, for which some of the $\mathcal{R}_c$, $\mathcal{R}_d$, $\mathcal{R}_f$, $\mathcal{R}_j$ functions introduced in Carlson's procedure are not defined [9].

In order to overcome these drawbacks, a semi-numerical modification of Urankar's integrals has been performed in our algorithm for field points (r, φ, z) located in these limit positions, consisting of numerical quadrature of one-dimensional integrals (4.3) in relative azimuthal coordinate. Elsewhere, the analytical approach has been used, resorting to Carlson's procedure for the computation of elliptic integrals. In the next section we discuss some numerical results after implementation of the integration schemes here introduced.

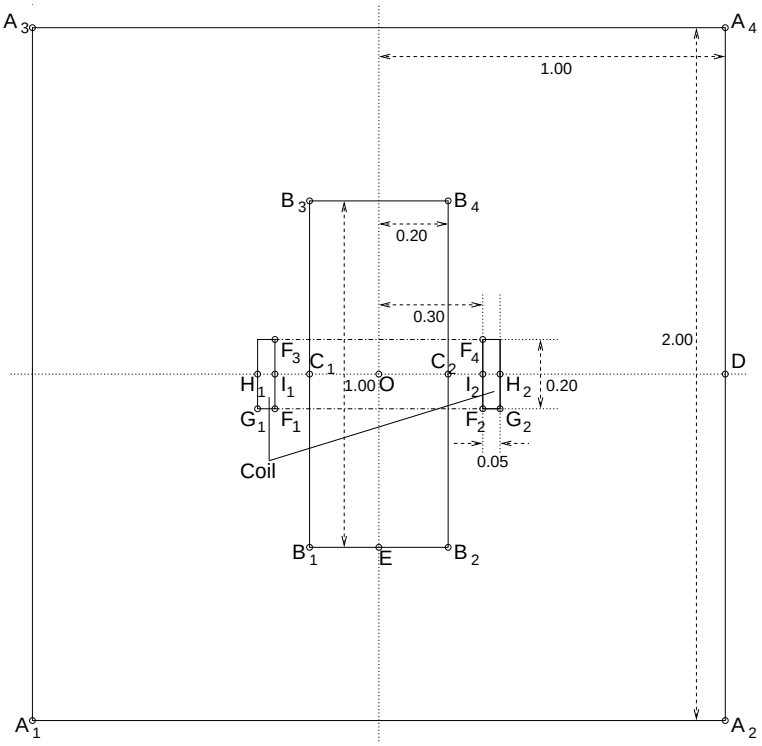

Figure 2: Axial section of the test domain (dimensions in meters)

5 Numerical examples

Among the several computation techniques of the Biot-Savart law above mentioned, numerical tests have been carried out, considering the following methods:

(a) finite volume integration with composite Gauss-Legendre quadrature on each volume (tetrahedron) inside the current-carrying conductor;

(b) composite trapezoidal integration of Urankar's one-dimensional integrals (4.3) with fixed angular step length;

(c) computation of Urankar's analytical expressions of Section 4, using Carlson's algorithm for the numerical estimation of elliptic integrals, and composite trapezoidal integration of Urankar's one-dimensional integrals for points located on the critic curves (called in the following the *modified Ur nk r's semi- n lytic l method*).

As a test case, values of a magnetostatic field $\mathbf{H}_s$ have been computed for points lying inside a cylindrical domain having radius $R = 1\,m$ and height $H = 2\,m$, where a stationary current flows along a circular toroidal winding with rectangular cross section, complete azimuthal width $2\,\pi$ radians, and inner/outer radii $R_1 = 0.3\,m$ and $R_2 = 0.35\,m$, respectively. The axis of the cylindrical geometry coincides with the axis of the coil, the center of the coil being located at the center of the domain. The current is constant in magnitude

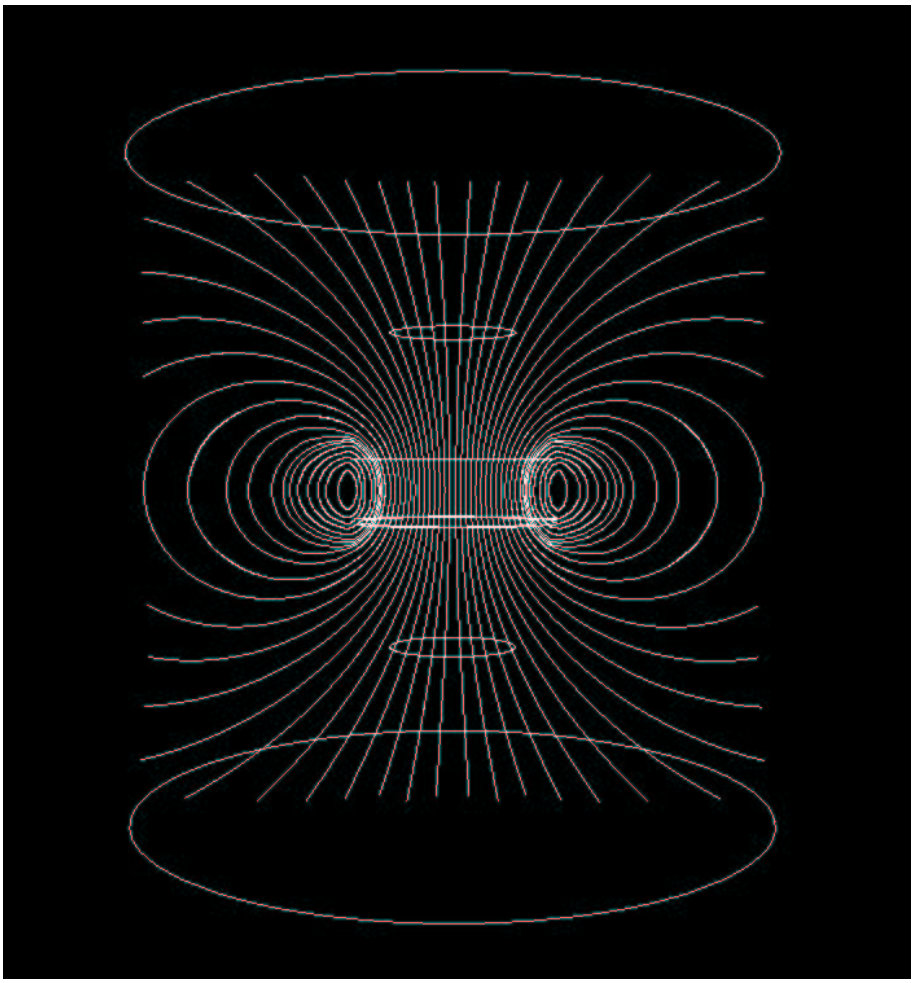

Figure 3: Streamlines of the magnetic field generated by a constant current in a circular coil with rectangular cross section

with density $J_s = 100\,A/m^2$, i.e. total intensity $1\,A$. To analyse results in different space regions, a subdomain is selected: a cylinder with radius $R_0 = 0.2\,m$ and height $H_0 = 1\,m$ having the same symmetry axis and the same center as the main domain and the coil winding.

Figure 2 shows a planar section of the domain and a selection of sample points located in various positions, chosen for a local evaluation of $\mathbf{H}_s$ (see Table 1). Figure 3 describes qualitatively the perfectly axisymmetric behaviour of the magnetostatic field generated by the current, computed by Urankar's semi-analytical method, showing the field streamlines along a planar section containing the symmetry axis.

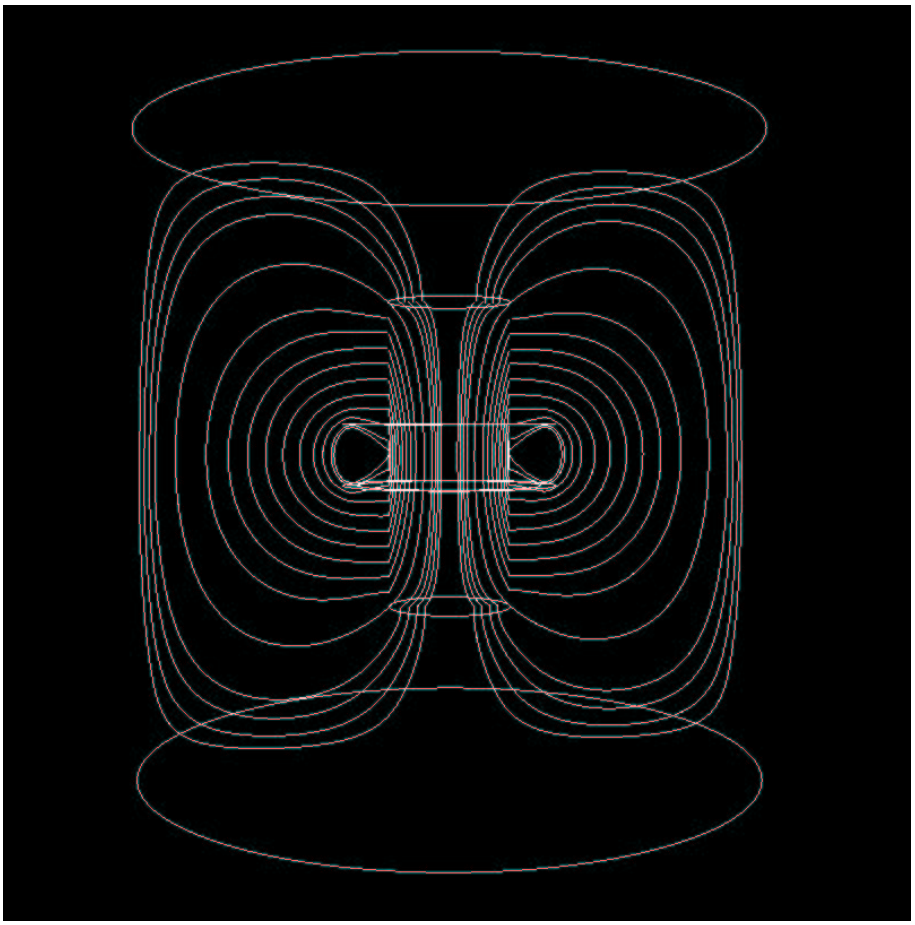

Figure 4: Streamlines of the total magnetic field in the material system iron/air associated to the test model

The magnetic field $\mathbf{H}_s$ generated by currents coincides with the total magnetic field in free space. $\mathbf{H}_s$ is by definition a "source" datum independent from the existence of background materials. On the other hand, when background materials are present also magnetization effects have to be included, according to (3.1). To see how the accuracy (or not) in the computation of the Biot-Savart law can affect results in complete electromagnetic problems requiring evaluation of all field contributions, $\mathbf{H}_s$ as well $\mathbf{H}_m$, we associate background materials to the initial model. As a possible choice, the small cylinder is an iron core inserted inside a coil winding made of copper, surrounded by air within the main cylindrical box. To evaluate the magnetization effects, the following values have been considered: $\mu_{r,Fe} = 10^4$ is the relative permeability of iron, $\mu_{r,Cu} = \mu_{r,air} = 1$ are the relative permeabilities of coil and air, respectively.

Figure 4 shows then the qualitative behaviour of the total magnetic field, due to the source field, as depicted in Figure 3, added up with induced magnetization due to the background materials. The field contribution due to magnetization has been computed from gradients of associated potentials, using a Galerkin finite element solution on a tetrahedral mesh of a Poisson problem with non-homogeneous Neumann/Dirichlet boundary and interface conditions [12]. In this model $\mathbf{H}_s$ plays the role of "source" in the differential equation (through its divergence) or implicit datum in the interface/boundary conditions (through computation of line integrals, or its normal component). Notice in Figure 4 the tangential discontinuity of the magnetic field streamlines at the interface iron/air, due to the jump of discontinuity of the relative magnetic permeability in the transition between iron and air.

To analyse in "global" sense the accuracy in the computation of the Biot-Savart law, quantities of physical significance can be evaluated in several subregions, for instance the magnetic energies. If the background material of a domain $\Omega \subseteq R^3$ has magnetic permeability μ, assuming that $\mathbf{B}$ is linearly related to $\mathbf{H}$, the total magnetic energy stored in Ω due to $\mathbf{H}$ is defined as

$$W_\Omega = \frac{1}{2}\int_\Omega \mathbf{B}\cdot\mathbf{H}\, d\mathbf{x} = \frac{1}{2}\mu_0 \int_\Omega \mu_r H^2\, d\mathbf{x}. \tag{5.1}$$

In a similar way, we can define on Ω the magnetic energy contribution due to source currents, depending only on $\mathbf{H}_s$, that is

$$W^0_\Omega = \frac{1}{2}\mu_0 \int_\Omega H_s^2\, d\mathbf{x}, \tag{5.2}$$

corresponding to the magnetic energy in free space.

To make our tests more significant, tests have been done on many points located in different positions inside all materials, either close or far from current-carrying regions. Notice that the Biot-Savart law generally has to be computed on a large number of field points, variously distributed in space. For instance, if $\mathbf{H}_s$ is required as a modelling datum for a successive finite element solution of boundary value problems, the points on which the source field has to be evaluated correspond to nodes of finite element triangulations associated to the space domain. In such a case a massive computation of 10^4-10^6 nodes can be requested, depending on accuracy requirements on the searched finite element solution.

Table 1 shows some values of $\mathbf{H}_s$ on the selection on field points shown in Figure 2. Columns 1 through 4 refer to finite volume Gauss-Legendre integration of type (a), using a 4-point rule on each tetrahedral volume, for increasing number of volumes in coils. The values computed by composite trapezoidal quadrature of Urankar's integrals are here obtained by choosing $h = 0.02$ as angular step length, i.e. about 314 subintervals (column 5). Finally, column 6 reports data obtained by the semi-analytical Urankar's method. Together with the already mentioned numerical integrations of type (b) for points located on

Pt.	Fin. Vol. *4pt-Gauss* 281 *vol.*	Fin. Vol. *4pt-Gauss* 1591 *vol.*	Fin. Vol. *4pt-Gauss* 6752 *vol.*	Fin. Vol. *4pt-Gauss* 39078 *vol.*	N. Urankar *trapez.rule* 314 *steps*	Urankar *semi-analyt.*
A_1	0.0147309	0.0146535	0.0147353	0.0147455	0.0147471	0.0147479
A_2	0.0147090	0.0147211	0.0147286	0.0147434	0.0147577	0.0147479
A_3	0.0147315	0.0147273	0.0147280	0.0147433	0.0147577	0.0147479
A_4	0.0147093	0.0146563	0.0147345	0.0147453	0.0147471	0.0147479
B_1	0.227632	0.226454	0.226977	0.227051	0.227081	0.227077
B_2	0.227567	0.226617	0.226955	0.227041	0.227118	0.227077
B_3	0.227663	0.226857	0.226904	0.227033	0.227118	0.227077
B_4	0.227575	0.226552	0.226924	0.227038	0.227081	0.227077
C_1	1.98978	1.94482	1.94353	1.94055	1.93924	1.93897
C_2	1.98764	1.94780	1.94225	1.94027	1.94024	1.93897
D	0.0293843	0.0294339	0.0294115	0.0294561	0.0295239	0.0294932
E	0.258566	0.257194	0.257579	0.257634	0.257673	0.257639
F_1	2.50560	2.44053	2.45220	2.50891	2.56669	2.56669
F_2	2.42779	2.47726	2.46863	2.51103	2.56381	2.56381
F_3	2.50758	2.42652	2.45312	2.50699	2.56669	2.56669
F_4	2.42657	2.48677	2.46863	2.50811	2.56381	2.56381
G_1	1.75404	1.68651	1.72674	1.77891	1.82984	1.82984
G_2	1.65583	1.69985	1.72091	1.77643	1.82685	1.82685
H_1	0.978923	1.14658	1.24033	1.29946	1.36610	1.34769
H_2	1.08817	1.14118	1.22937	1.29565	1.36135	1.34769
I_1	2.39006	2.70197	2.77251	2.85931	2.93927	2.94681
I_2	2.57858	2.79818	2.78436	2.85431	2.93520	2.94681
O	0.000000	0.000000	0.000000	0.000000	0.000000	0.000000

Table 1: Values in magnitude of the source magnetic field $\mathbf{H}_s$ on sample points

the critic curves, or the computation of elliptic integrals via Carlson's algorithm, a further numerical contribution in method (c) consists of composite Gaussian quadrature of integral $\Im(\alpha)$ (12-point rule).

As expected, Table 1 shows that the numerical results obtained from composite trapezoidal quadrature of Urankar's one-dimensional integrals (4.3) are closer to values computed by Urankar's semi-analytical method than to values computed by finite volume integration, even in the case of the finest decomposition. Urankar's method (c) stands out in its perfectly axisymmetric results, as expected by azimuthal independence of formulas when the coil has a complete angular width 2π radians. As concerns the composite trapezoidal integration in method (b), a refinement in the step size from $h = 0.02$ to $h = 0.001$, does not affect the accuracy of field values up to the 5th significant decimal digit. As concerns

Method	W^0_{tot}	W^0_{coil}	W^0_{cyl}
Fin.Vol. (*4pt-Gauss*, 281)	$3.4743 \cdot 10^{-7}$	$2.2061 \cdot 10^{-8}$	$7.6728 \cdot 10^{-8}$
N.Urankar (*trapez. rule*)	$3.6275 \cdot 10^{-7}$	$2.5614 \cdot 10^{-8}$	$7.4229 \cdot 10^{-8}$
Urankar (*semi-analytical*)	$3.6275 \cdot 10^{-7}$	$2.5703 \cdot 10^{-8}$	$7.4206 \cdot 10^{-8}$
Fin.Vol. (*4pt-Gauss*, 1310)	$3.5896 \cdot 10^{-7}$	$2.6200 \cdot 10^{-8}$	$7.7884 \cdot 10^{-8}$
N.Urankar (*trapez. rule*)	$3.7305 \cdot 10^{-7}$	$2.9370 \cdot 10^{-8}$	$7.7308 \cdot 10^{-8}$
Urankar (*semi-analytical*)	$3.7307 \cdot 10^{-7}$	$2.9514 \cdot 10^{-8}$	$7.7285 \cdot 10^{-8}$
Fin.Vol. (*4pt-Gauss*, 4792)	$3.6736 \cdot 10^{-7}$	$3.0496 \cdot 10^{-8}$	$7.8359 \cdot 10^{-8}$
N.Urankar (*trapez. rule*)	$3.7592 \cdot 10^{-7}$	$3.2582 \cdot 10^{-8}$	$7.8284 \cdot 10^{-8}$
Urankar (*semi-analytical*)	$3.7587 \cdot 10^{-7}$	$3.2680 \cdot 10^{-8}$	$7.8260 \cdot 10^{-8}$
Fin.Vol. (*4pt-Gauss*, 18910)	$3.7317 \cdot 10^{-7}$	$3.3693 \cdot 10^{-8}$	$7.8474 \cdot 10^{-8}$
N.Urankar (*trapez. rule*)	$3.7704 \cdot 10^{-7}$	$3.4764 \cdot 10^{-8}$	$7.8545 \cdot 10^{-8}$
Urankar (*semi-analytical*)	$3.7717 \cdot 10^{-7}$	$3.4989 \cdot 10^{-8}$	$7.8521 \cdot 10^{-8}$
Fin.Vol. (*4pt-Gauss*, 35620)	$3.7462 \cdot 10^{-7}$	$3.4453 \cdot 10^{-8}$	$7.8642 \cdot 10^{-8}$
N.Urankar (*trapez. rule*)	$3.7748 \cdot 10^{-7}$	$3.5255 \cdot 10^{-8}$	$7.8734 \cdot 10^{-8}$
Urankar (*semi-analytical*)	$3.7764 \cdot 10^{-7}$	$3.5491 \cdot 10^{-8}$	$7.8710 \cdot 10^{-8}$

Table 2: Convergence of source magnetic energies computed by several methods (values in Joule)

W^0_{tot} (Vol.Int.)	W^0_{coil} (Vol.Int.)	W^0_{cyl} (Vol.Int.)
$3.7843 \cdot 10^{-7}$ (606158)	$3.6005 \cdot 10^{-8}$ (131202)	$7.8760 \cdot 10^{-8}$ (222389)
$3.7875 \cdot 10^{-7}$ (1582813)	$3.6006 \cdot 10^{-8}$ (132100)	$7.8813 \cdot 10^{-8}$ (892809)

Table 3: Sharp estimates of the source magnetic energies computed by the modified Urankar's semi-analytical method (in Joule)

the finite volume Gauss-Legendre integration in method (a), values are not sufficiently accurate for coarse volume subdivisions of the coil. When refining the volume subdivision, a higher accuracy is reached, the values converge towards the expected axisymmetric behaviour and draw near to values obtained by methods (b) and (c), nevertheless results are not very accurate in points close to the source region. For the finest finite volume subdivision, the relative errors are approximately $1 \sim 1.5 \cdot 10^{-4}$ in the most remote positions with respect to the source region, approximately $1 \cdot 10^{-3}$ in the geometry core (the small cylinder) and only $2 \sim 3 \cdot 10^{-2}$ near and inside the source region.

Global results are shown in Table 2, which reports estimates of the source magnetic energies W^0 in the whole domain, the current-carrying conductor and the central cylindrical core, depending on the method (a), (b) or (c) used for the computation of $\mathbf{H}_s$. The reported values for method (b), in this Table and in the successive ones, refer to a step size $h = 0.02$ in the composite trapezoidal integration. The estimation of W^0 is based on

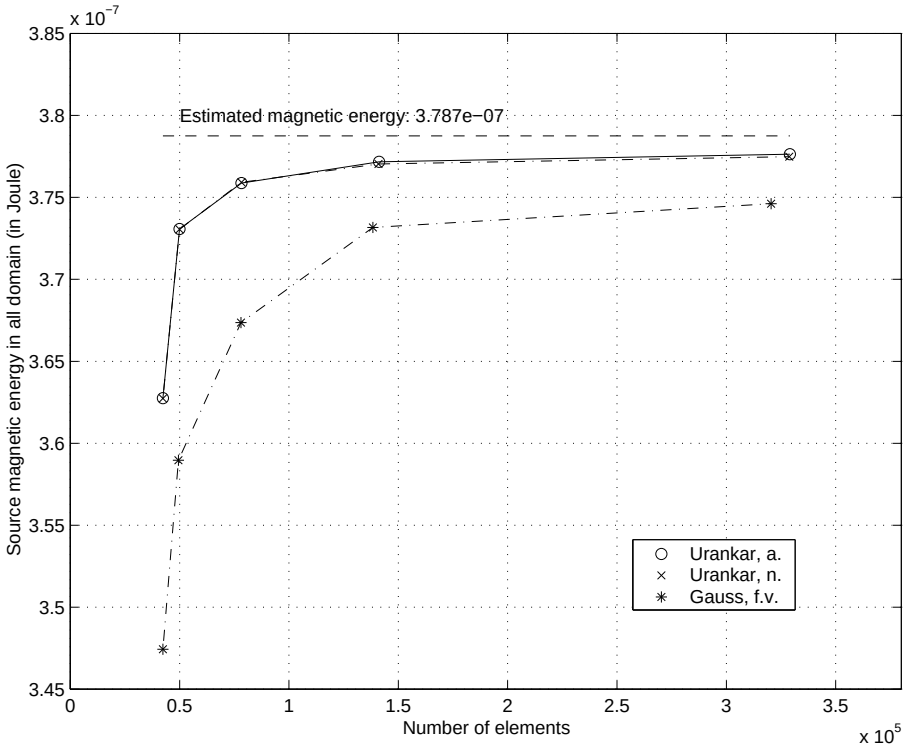

Figure 5: Trend of the source magnetic energy in free space (global domain)

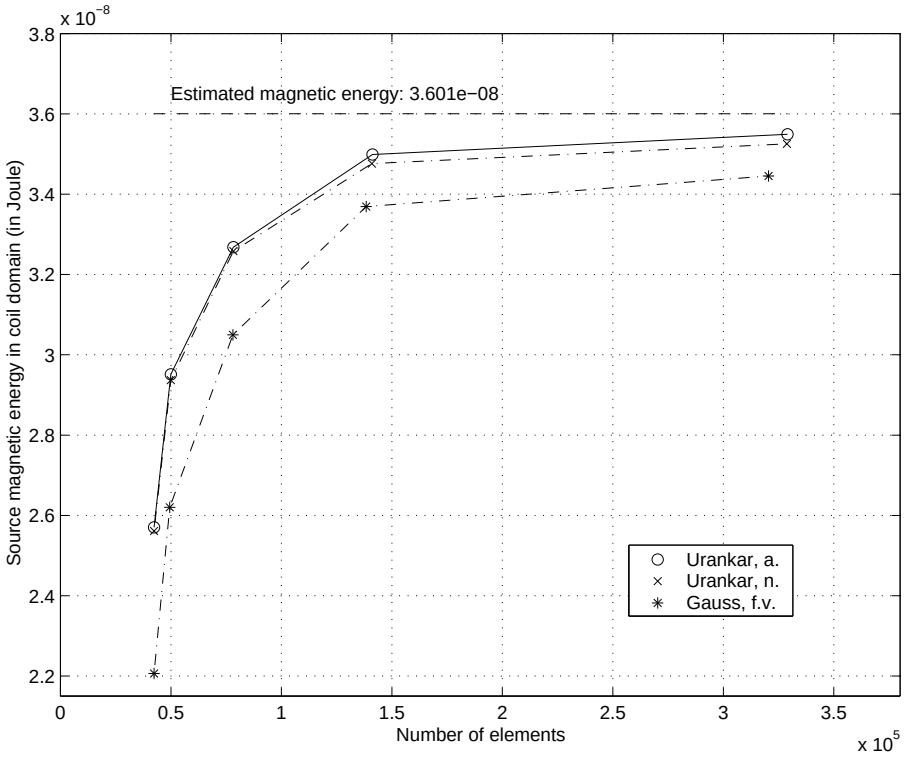

Figure 6: Trend of the source magnetic energy in free space (coil)

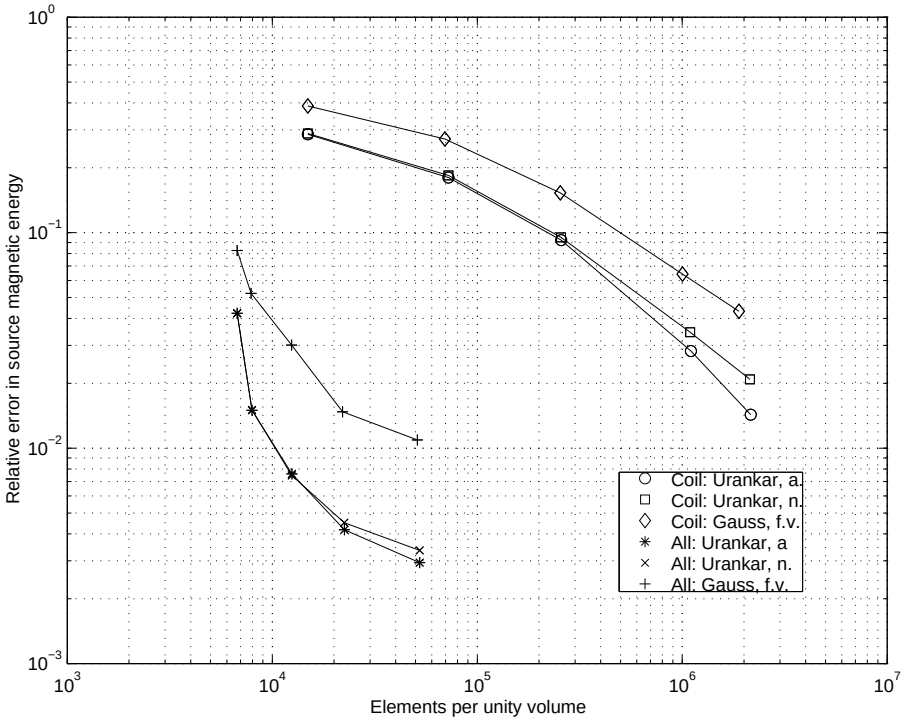

Figure 7: Comparison in logarithmic scale of relative errors in source magnetic energy

a composite 1-point volume quadrature of integral (5.2), in which the volumes are tetrahedra. The values are grouped together for each level of accuracy in the numerical integration of (5.2), i.e. by considering the same number of subdomains per region (up to an error of 1%), for increasing number of subdomains. Table 3 reports sharp estimates obtained by Urankar's method (c), considering a more accurate estimation of energy's integral (the number of integration subdomains is specified). Figures 5 and 6 show qualitatively the trend of convergence of source energies for methods (a), (b) and (c), in the global domain and the coil region respectively, towards the "best" estimates in Table 3.

For a qualitative error analysis, see Figures 8 and 9 describing relative errors of source magnetic energies, in the global domain and the source region respectively, considering the same level of accuracy in the numerical estimation of energy's integral. Figure 7 describes in logarithmic scale relative error curves for the global domain and the current-carrying conductor.

Numbers and graphics confirm even in global sense a better reliability of methods (b) and (c) based on Urankar's expressions with respect to finite volume integration (a). For all three methods, a higher accuracy is obtained in regions far from current-carrying conductors. This depends, evidently, on the singularity of type $O(|\mathbf{r}-\mathbf{r}'|^{-3})$ in the integrand function of the Biot-Savart law, not negligible when the field points $\mathbf{r}$ draw near to source

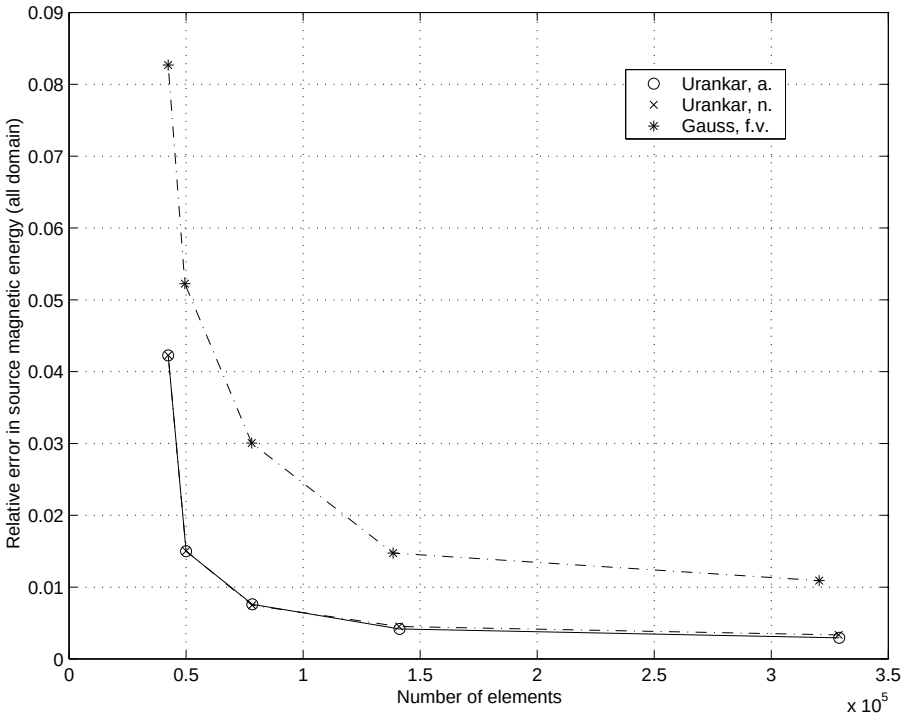

Figure 8: Relative errors of the source magnetic energy in free space (global domain)

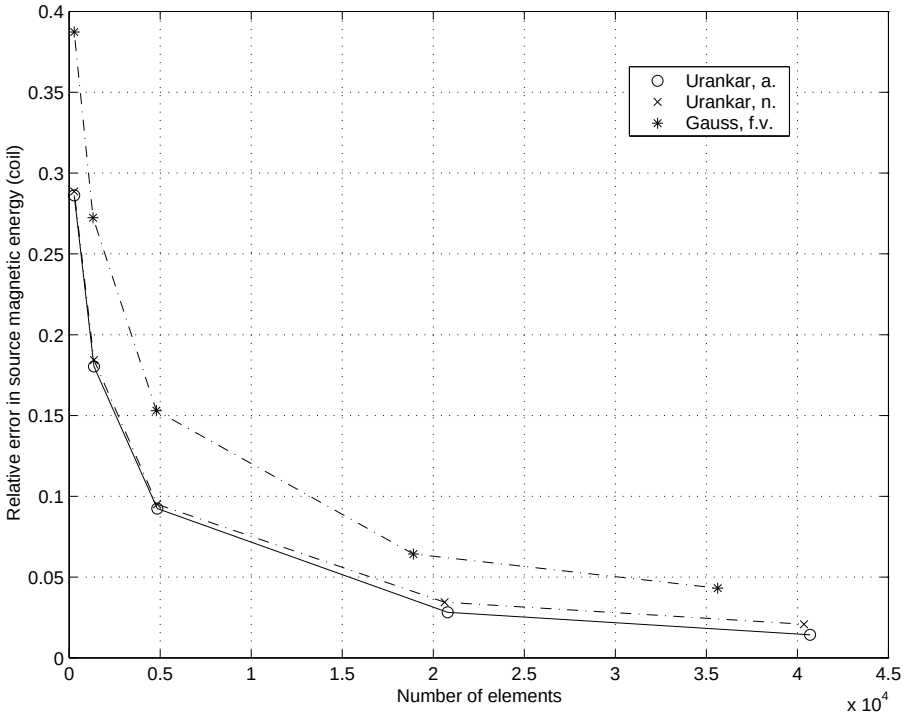

Figure 9: Relative errors of the source magnetic energy in free space (coil)

Method	W_{air}	W_{iron}	W_{coil}
Fin.Vol. (*4pt-Gauss, 281*)	$9.2239 \cdot 10^{-7}$	$5.3383 \cdot 10^{-10}$	$2.2369 \cdot 10^{-8}$
N.Urankar (*trapez. rule*)	$9.3381 \cdot 10^{-7}$	$5.3179 \cdot 10^{-10}$	$2.4003 \cdot 10^{-8}$
Urankar (*semi-analytical*)	$9.3346 \cdot 10^{-7}$	$5.3178 \cdot 10^{-10}$	$2.3960 \cdot 10^{-8}$
Fin.Vol. (*4pt-Gauss, 1591*)	$9.0936 \cdot 10^{-7}$	$4.9087 \cdot 10^{-10}$	$2.7188 \cdot 10^{-8}$
N.Urankar (*trapez. rule*)	$9.1965 \cdot 10^{-7}$	$4.9041 \cdot 10^{-10}$	$2.9404 \cdot 10^{-8}$
Urankar (*semi-analytical*)	$9.1946 \cdot 10^{-7}$	$4.9039 \cdot 10^{-10}$	$2.9544 \cdot 10^{-8}$
Fin.Vol. (*4pt-Gauss, 6752*)	$9.0935 \cdot 10^{-7}$	$4.8577 \cdot 10^{-10}$	$3.1523 \cdot 10^{-8}$
N.Urankar (*trapez. rule*)	$9.1406 \cdot 10^{-7}$	$4.8560 \cdot 10^{-10}$	$3.3017 \cdot 10^{-8}$
Urankar (*semi-analytical*)	$9.1395 \cdot 10^{-7}$	$4.8558 \cdot 10^{-10}$	$3.3093 \cdot 10^{-8}$
Fin.Vol. (*4pt-Gauss, 39078*)	$9.0954 \cdot 10^{-7}$	$4.8283 \cdot 10^{-10}$	$3.4550 \cdot 10^{-8}$
N.Urankar (*trapez. rule*)	$9.1118 \cdot 10^{-7}$	$4.8285 \cdot 10^{-10}$	$3.5244 \cdot 10^{-8}$
Urankar (*semi-analytical*)	$9.1109 \cdot 10^{-7}$	$4.8283 \cdot 10^{-10}$	$3.5283 \cdot 10^{-8}$

Table 4: Convergence of total magnetic energies computed by several methods (values in Joule)

	W_{air}	W_{iron}	W_{coil}
U.	$9.100 \cdot 10^{-7}$ (599025)	$4.778 \cdot 10^{-10}$ (37677)	$3.578 \cdot 10^{-8}$ (131294)
Ref.	$9.081 \cdot 10^{-7}$	$4.802 \cdot 10^{-10}$	$3.581 \cdot 10^{-8}$

Table 5: Reference values of the total magnetic energy (in Joule) computed by the modified Urankar's semi-analytical method (U) and least-squares FEM solution (Ref.)

points $\mathbf{r}'$. This aspect is especially evident for method (a). Because of such singularity, for instance, an extremely sharp volume subdivision of the coil in the finite volume integration, although giving a good accuracy far from the coil, would not guarantee a high accuracy close to it, since values would not be convergent as the volume size tends to zero. However, in practical computations, this critic level consisting of a "too fine" volume subdivision is never reached, and the values are still shown to converge even inside/near current-carrying conductors, as confirmed by Tables 1 and 2.

Finally, iron, copper and air have been considered as background materials for a total field evaluation including magnetization effects. Except for the integration of the Biot-Savart law through methods (a), (b) or (c), the other numerical contributions have been *ll* performed in the same way (here, the above mentioned Galerkin finite element solution for associated potentials, as well as the numerical integration of total energy's integral). Results are shown in Table 4, which reports for methods (a), (b) and (c) the estimates of the total magnetic energy W in air, iron and coil, grouped together for the same level of accuracy in energy's integral estimation (the number of integration subdomains is specified). Table 5 reports values estimated by Urankar's semi-analytical method using a particularly

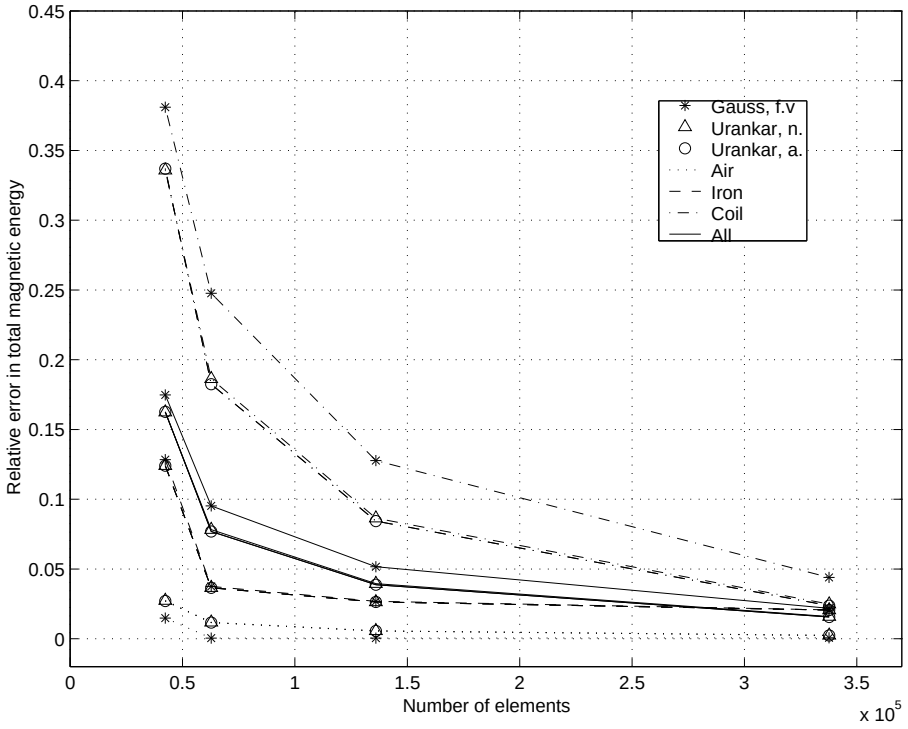

Figure 10: Comparison of relative errors in total magnetic energy among various materials

fine volume subdivision to compute the total energy's integral (with specified number of subdomains), in comparison with reference values. The latter have been computed from a piecewise quadratic least-squares finite element solution of static Maxwell's equations in field formulation, not resorting to any estimation of the Biot-Savart law [5]. For an error analysis see Figure 10, giving a simultaneous representation of the relative errors in total magnetic energies on all three materials and on the global domain, considering the three integration methods of the Biot-Savart law. Even in this case including magnetization effects, Urankar's semi-analytical method, as well as a complete numerical quadrature of Urankar's integrals, confirms a higher accuracy of values in current-carrying regions compared to values computed by the finite volume approximation. The latter shows rather good results in regions not containing currents.

To conclude, Table 6 reports an estimation of computational times to evaluate $\mathbf{H}_s$ on a large number of field points distributed in the overall domain, with Figure 11 describing the performance trend in logarithmic scale. Computations have been performed on a Sun-Solaris Unix station, 2048 Mb memory. Notice that the semi-analytical Urankar's scheme is a great deal faster than the other two methods. Concerning finite volume Gaussian schemes, in fact, iterations have to be performed on all coil volumes. Just to give an idea through a coarse estimation on a convex and simple geometry like the one considered

No. points	7970	11613	24233	59000
Fin.Vol.	14”	1’52”	16’45”	3 h 28’25”
(*4pt-Gauss*)	(40%)	(42%)	(41%)	(37%)
N.Urankar	10’23”	15’47”	29’40”	1 h 12’16”
(*trapez. rule*)	(46%)	(47%)	(46%)	(48%)
Urankar	13”	23”	37”	1’37”
(*semi-analytical*)	(21%)	(26%)	(27%)	(26%)

Table 6: Performance analysis: estimation of computational times (with percentage of CPU usage)

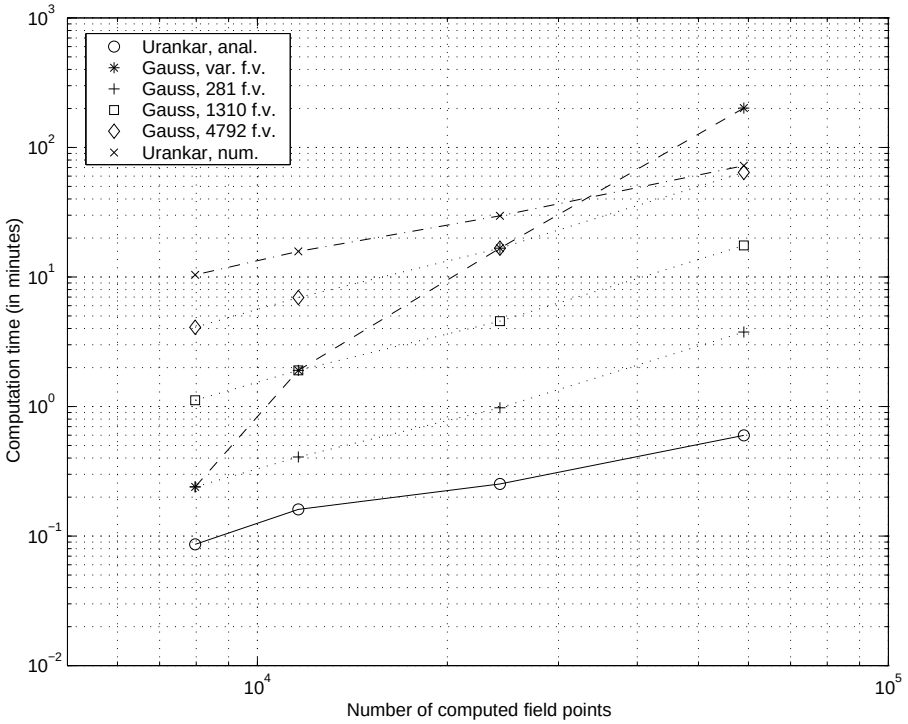

Figure 11: Trend of computational times in logarithmic scale

in Figure 2, if the volumes coincide with the elements inside the coil belonging to a 3D triangulation used for a FEM computation, there can be a number of tetrahedra of orders $10^2 - 10^5$ to be considered, each of them giving an elemental contribution on $10^4 - 10^6$ field points (FEM nodes) approximately, the higher number it is the finer the FEM triangulation is [12].

The efficiency of the semi-analytical Urankar's method on coils is evident in terms of accuracy and computational time. Nevertheless, for current-carrying geometries not described by simple shapes like circular coils with rectangular (or polygonal) cross section (or straight bars, see Appendix in [22]) the finite volume approximation still would remain a fair alternative.

An application of the Biot-Savart law and further numerical examples can be found in [12], where magnetic field computations have been performed by choosing the modified Urankar's semi-analytical method. In such work test models have been considered for a more extended study, involving both modelling aspects (computation of the Biot-Savart law is, in fact, one of them) and adaptive finite element analysis.

6 Conclusions and future work

Numerical and semi-analytical methods have been here proposed to compute the magnetic field intensity due to imposed currents, based on integration of the Biot-Savart law. When the current-carrying region is a circular coil with rectangular cross section, Urankar's semi-analytical formulas can be used. Some corrections have been done with respect to the original expressions, and limit values have been specified for field points located in particular space positions. A modified semi-analytical method has been proposed, efficient for a massive computation on a large number of field points, combining semi-analytical expressions with numerical quadrature of one-dimensional integrals in relative azimuthal coordinate. For complex-shaped current-carrying conductors, a numerical integration of the Biot-Savart law needs to be performed, and a finite volume approximation is proposed, based on a composite three-dimensional Gauss-Legendre integration over tetrahedral subdomains of the conductors.

Some test cases have been considered to make a comparison between Urankar's approach, both the modified semi-analytical method and a complete numerical treatment of one-dimensional Urankar's integrals, with a finite volume approximation by composite Gauss-Legendre quadrature. Results confirm averagely the higher accuracy of Urankar's semi-analytical method. Even a numerical treatment of Urankar's integrals gives better results than finite volume integrations. In all cases, a higher accuracy is obtained in regions far from current-carrying conductors, as expected because of a singularity of type $O(|\mathbf{r} - \mathbf{r}'|^{-3})$. On the other hand, a finite volume integration performed on a very fine vol-

ume subdivision gives good results as well. The problem in the finite volume approximation is, rather, the not significant accuracy in regions close to current-carrying conductors and, above all, the high computational cost and time. Even numerical integration of Urankar's integral is quite time consuming. On the contrary, Urankar's semi-analytical scheme is fast and efficient. The main drawback in Urankar's approach is rather the fact that it cannot be applied to more general conducting geometries than unions of coils or bars with polygonal cross section.

The widespread need and utilization of the Biot-Savart law in electromagnetic models suggests possible tasks for future work, not only specific for magnetic field computation but also interesting from a mathematical point of view, somehow training to develop methods for the numerical integration of volume integrals having singularities or complex-shaped integration domains, as they appear in many engineering problems.

Concerning the computation of the Biot-Savart law for electromagnetic applications, a possible task for a future work is to compare Urankar's techniques with Ciric's surface source method, another efficient method that can be applied to coils with polygonal cross section. Anyway, because of the complexity of current-carrying geometries on real electromagnetic devices, it makes sense to focus also on some improvement of finite volume integration techniques, whose idea can be extended to other three-dimensional integration problems. For instance, modified weighted 3D Gaussian integration schemes could be introduced, for significant volume shapes. Such schemes could be tested by choosing the weights properly so that the contribution of the singularity appearing in the integrand function of the Biot-Savart law is reduced with respect to the classical Gauss-Legendre quadrature. Various volume shapes can be considered. Using tetrahedral shapes as finite volumes, for instance, can be convenient when integration has to be combined with a finite element solution of associated boundary value problems on 3D triangular meshes.

Acknowledgements

The author wishes to thank particularly Prof. Claes Johnson for his scientific and moral support, and for his hospitality at Chalmers Finite Element Center of Chalmers University of Technology in Göteborg, Sweden, together with all the people of the center and the Department of Mathematics of Chalmers University and Göteborg University. Among them, she is indebted to Klas Samuelsson, for his precious teaching and help in questions concerning programming and some numerical aspects, and to Rickard Bergström and Niklas Ericsson of the same department for their help in C++ and Unix matters.

She is also grateful to Alessandro Castagnini of ABB Ricerca in Milano, Italy, Piergiorgio Alotto of the Department of Electrical Engineering in Genova University, Italy, and Andrea Bertoni of TechnoSoft s.a.s. in Genova for their help and precious consultancy.

This work has been financially supported by the National Research Council (CNR) of Italy through research fellowship, grant n. 203.01.70 for Mathematical Sciences.

References

[1] M. Abramowitz, I.A. Stegun, *H ndbook of M them tic l Functions*, Dover Publications, New York (1968)

[2] B. Azzerboni, E. Cardelli, M. Raugi, A. Tellini, G. Tina, *M gnetic field ev lu tion for thick nnul r conductors*, IEEE Trans. Magn. 29, 2090-2094 (1993)

[3] S. Babic, Z. Andjelic, B. Krstajic, S. Salon, *An lytic l c lcul tion of the 3D m gnetost tic field of thoroid l conductor with rect ngul r cross section*, IEEE Trans. Magn. 24, 3162-3164 (1988)

[4] J.J. Barton, L.R. Nackman, *Scientific nd engineering C++*, Addison-Wesley (1997)

[5] R. Bergström, *Le st squ res finite element methods for electrom gnetic pplic tions*, Lic. Thesis, Dept. Mathematics, Chalmers University of Technology, Göteborg (2000)

[6] R. Bulirsch, *An extension of the B rtky-tr nsform tion to incomplete elliptic integr ls of the third kind*, Num. Math. 13, 266-284 (1969)

[7] R. Bulirsch, *Numeric l c lcul tions of elliptic integr ls nd elliptic functions. III*, Num. Math 13, 305-315 (1969)

[8] P.F. Byrd, M.D. Friedman, *H ndbook of Elliptic Integr ls for Engineers nd Scientists*, Springer, New York (1971)

[9] B.C. Carlson, *Computing elliptic integr ls by duplic tion*, Num. Math. 33, 1-16 (1979)

[10] D.K. Cheng, *Field nd W ve Electrom gnetics*, Addison-Wesley (1983)

[11] I.R. Ciric, *Formul s for the M gnetic field of polygon l cross section current coils*, IEEE Trans. Magn. 28, 1064-1067 (1992)

[12] M. Fontana, *Ad ptive finite element comput tion of 3D m gnetost tic problems in potenti l formul tion*, Finite Element Center Preprint, Chalmers University of Technology, Göteborg (2001, to appear)

[13] W.H. Hayt, *Engineering Electrom gnetics*, McGraw-Hill (1987)

[14] M. Krizek, P. Neittaanmäki, *M them tic l nd Numeric l Modelling in Electric l Engineering*, Kluwer Academic Publishers (1996)

[15] B. Krstajic, Z. Andjelic, S. Milojkovic, S. Babic, S. Salon, *Nonline r 3D m gnetost tic field c lcul tion by the integr l equ tion method with surf ce nd volume m gnetic ch rges*, IEEE Trans. Magn. 28, 1088-1091 (1992)

[16] E.H. Neville, *J cobi n Elliptic Functions*, Oxford Clarendon Press (1951)

[17] W.H. Press, S.A. Teukolsky, W.T. Vetterling, B.P. Flannery, *Numeric l recipes in C*, Cambridge University Press (1992)

[18] M. Touma Holmberg, *Three-dimension l finite element comput tion of eddy currents in synchronous m chines*, Ph.D. Thesis, Dept. Electric Power Engineering, Chalmers University of Technology, Göteborg (1998)

[19] C.W. Trowbridge, *An Introduction to Computer Aided Electrom gnetic An lysis*, J. Wiley and Sons (1992)

[20] L.U. Urankar, *Vector potenti l nd m gnetic field of current-c rrying finite rc segment in n lytic l form. P rt I: Fil ment pproxim tion*, IEEE Trans. Magn. 16, 1283-1288 (1980)

[21] L.U. Urankar, *Vector potenti l nd m gnetic field of current-c rrying finite rc segment in n lytic l form. P rt II: Thin sheet pproxim tion*, IEEE Trans. Magn. 18, 911-917 (1982)

[22] L.U. Urankar, *Vector potenti l nd m gnetic field of current-c rrying finite rc segment in n lytic l form. P rt III: Ex ct comput tion for rect ngul r cross section*, IEEE Trans. Magn. 18, 1860-1867 (1982)

[23] L.U. Urankar, *Vector potenti l nd m gnetic field of current-c rrying finite rc segment in n lytic l form. P rt IV: Gener l three-dimension l current density*, IEEE Trans. Magn. 20, 2145-2150 (1984)

[24] L.U. Urankar, *Vector potenti l nd m gnetic field of current-c rrying finite rc segment in n lytic l form. P rt V: Polygon cross section*, IEEE Trans. Magn. 26, 1171-1180 (1990)

[25] L.U. Urankar, *Comp ct extended lgorithms for elliptic integr ls in electrom gnetic field nd potenti l comput tions. P rt I: Elliptic integr ls of the first nd second kind with extended integr tion r nge*, IEEE Trans. Magn. 27, 4338-4342 (1991)

[26] L.U. Urankar, *Comp ct extended lgorithms for elliptic integr ls in electrom gnetic field nd potenti l comput tions. P rt II: Elliptic integr ls of the third kind with extended integr tion r nge*, IEEE Trans. Magn. 30, 1236-1241 (1991)

Chalmers Finite Element Center Preprints

2000–01 *Adaptive Finite Element Methods for the Unsteady Maxwell's Equations*
Johan Hoffman

2000–02 *A Multi-Adaptive ODE-Solver*
Anders Logg

2000–03 *Multi-Adaptive Error Control for ODEs*
Anders Logg

2000–04 *Dynamic Computational Subgrid Modeling* (Licentiate Thesis)
Johan Hoffman

2000–05 *Least-Squares Finite Element Methods for Electromagnetic Applications* (Licentiate Thesis)
Rickard Bergström

2000–06 *Discontinuous Galerkin Methods for Incompressible and Nearly Incompressible Elasticity by Nitsche's Method*
Peter Hansbo and Mats G. Larson

2000–07 *A Discountinuous Galerkin Method for the Plate Equation*
Peter Hansbo and Mats G. Larson

2000–08 *Conservation Properties for the Continuous and Discontinuous Galerkin Methods*
Mats G. Larson and A. Jonas Niklasson

2000–09 *Discontinuous Galerkin and the Crouzeix-Raviart element: Application to elasticity*
Peter Hansbo and Mats G. Larson

2000–10 *Pointwise A Posteriori Error Analysis for an Adaptive Penalty Finite Element Method for the Obstacle Problem*
Donald A. French, Stig Larson and Ricardo H. Nochetto

2000–11 *Global and Localised A Posteriori Error Analysis in the Maximum Norm for Finite Element Approximations of a Convection-Diffusion Problem*
Mats Boman

2000–12 *A Posteriori Error Analysis in the Maximum Norm for a Penalty Finite Element Method for the Time-Dependent Obstacle Problem*
Mats Boman

2000–13 *A Posteriori Error Analysis in the Maximum Norm for Finite Element Approximations of a Time-Dependent Convection-Diffusion Problem*
Mats Boman

2001–01 *A Simple Nonconforming Bilinear Element for the Elasticity Problem*
Peter Hansbo and Mats G. Larson

2001–02 *The $\mathcal{LL}^*$ Finite Element Method and Multigrid for the Magnetostatic Problem*
Rickard Bergström, Mats G. Larson, and Klas Samuelsson

2001–03 *The Fokker-Planck Operator as an Asymptotic Limit in Anisotropic Media*
Mohammad Asadzadeh

2001–04 *A Posteriori Error Estimation of Functionals in Elliptic Problems: Experiments*
Mats G. Larson and A. Jonas Niklasson

2001–05 *A Note on Energy Conservation for Hamiltonian Systems Using Continuous Time Finite Elements*
Peter Hansbo

2001–06 *Stationary Level Set Method for Modelling Sharp Interfaces in Groundwater Flow*
Nahidh Sharif and Nils-Erik Wiberg

2001–07 *Integration methods for the calculation of the magnetostatic field due to coils*
Marzia Fontana

These preprints can be obtained from

`www.phi.chalmers.se/preprints`